FLAP-LAG DYNAMICS OF HINGELESS HELICOPTER BLADES AT MODERATE AND HIGH ADVANCE RATIOS

P. Friedmann
Assistant Professor

and

L.J. Silverthorn[*]
Research Assistant
Mechanics and Structures Department
School of Engineering and Applied Science
University of California, Los Angeles

Abstract

Equations for large amplitude coupled flap-lag motion of a hingeless elastic helicopter blade in forward flight are derived. Only a torsionally rigid blade exicted by quasi-steady aerodynamic loads is considered. The effects of reversed flow together with some new terms due to forward flight are included. Using Galerkin's method the spatial dependence is eliminated and the equations are linearized about a suitable equilibrium position.

The resulting system of equations is solved using multivariable Floquet-Liapunov theory, and the transition matrix at the end of the period is evaluated by two separate methods. Results illustrating the effects of forward flight and various important blade parameters on the stability boundaries are presented.

Notation

a	Two dimensional lift curve slope
$\bar{A}$	Tip loss coefficient
$\underset{\sim}{A}$	Periodic matrix with elements A_{ij}, defined in Appendix B
A_{Fi}, A_{Li}	Generalized aerodynamic force for i^{th} flap and lag mode respectively
$\bar{A}_{Fi}, \bar{A}_{Li}$	Same as above, in reverse and mixed flow regions.
b	Semi-chord nondimensionalized with respect to R
$\bar{B}$	Tip loss coefficient
$\bar{B}^i$	Generalized masses defined in Appendix A
C_T	Thrust coefficient
$\underset{\sim}{C}$	Constant matrix
C_{do}	Profile drag coefficient

$C(k)$	Theodorsen's lift deficiency function
e_1	Defined in Fig. 1
$F_{C1}, E_{C2}, \bar{E}^{\bar{b}}_{ik}, \bar{E}^b_{im}, \bar{E}^{cs}_{im}, \bar{E}^{cs}_{ik}$	Terms associated with elastic coupling defined in Appendix A
$(EI)_y$	Stiffness for flapwise bending
$(EI)_z$	Stiffness for inplane of rotation bending
F^i	Flap coefficients defined in Appendix A
g_k	Generalized coordinate, k^{th} normal flapping mode
g_k^o	Static value of g_k in hover
Δg_k	Perturbation in g_k about g_k^o
g_{SF}, g_{SL}	Viscous structural damping in flap and lag respectively
h_m	Generalized coordinate, m^{th} normal inplane mode
h_k^o	Static value of h_k in hover
Δh_k	Perturbation in h_k about h_k^o
$i = \sqrt{-1}$	
$\underset{\sim}{i}, \underset{\sim}{j}, \underset{\sim}{k}$	Unit vectors in x,y and z directions (Fig. 1)
I_b	Mass moment of inertia in flap, defined in Appendix A
$\underset{\sim}{I}$	Unit matrix
ℓ	Length of blade capable of elastic deflection
L_y, L_z	Aerodynamic load per unit length in the y and z directions respectively
L^i	Lag coefficients, defined in Appendix A
m	Mass of blade per unit length

[*]Presently, Dynamics Engineer, Hughes Helicopter Company, Culver City, California.

55

M,N	Number of modes in lag and flap respectively	β_D	Droop, built in angle of the undeformed position of the blade measured from the feathering axis (Fig. 1)
$\overline{M}_{F1}, \overline{M}_{Li}$	Generalized mass for the ith flap and lag mode respectively, defined in Appendix A	β_P	Preconing, inclination of the feathering axis w.r.t. the hub plane measured in a vertical plane
$(\overline{M}_\eta)_{ik\ell}, (\overline{M}_\gamma)_{imr}$	Defined in Appendix A		
P_x, P_y, P_z	Resultant total loading per unit length in the x,y and z direction respectively	γ	Lock number ($\gamma = 2\rho_A bR^5 a/I_b$) for normal flow
$\overline{P}_{ikm}$	Defined in Appendix A	γ_m	m^{th} inplane bending mode
$\underset{\sim}{P}(t)$	Periodic matrix	ϵ_D	Symbolic quantity having the same order of magnitude like the displacements v and w
R	Blade radius		
$\underset{\sim}{R}$	Constant matrix used in Floquet-Liapunov theorem	ζ_k	Real part of the kth characteristic exponent
$\underset{\sim}{Q}$	Constant matrix	η_k	k^{th} flapwise bending mode
T	Common nondimensional period	η_{SF_1}, η_{SL_1}	Viscous structural damping coefficients defined in Appendix A
u,v,w	x,y and z displacement of a point on the elastic axis of the blade	θ	Collective pitch angle measured from x-y plane
U_P	Component of air velocity w.r.t. the blade at station x perpendicular to x-y plane (hub plane), positive down	θ_C	Critical value of collective pitch at which the linearized coupled flap-lag system becomes unstable in hover
U_T	Same as above, in the x-y plane, tangent to a circle having a radius x	λ	Inflow ratio, induced velocity over disk, positive down, non-dimensionalized w.r.t. $R\Omega$
v_e, v_{eo}	Elastic part of the displacement of a point on the elastic axis of the blade parallel to hub plane, (see Fig. 1), subscript o denotes the static equilibrium value	$\underset{\sim}{\lambda}$	Diagonal matrix, containing eigenvalues λ_k of R
		$\underset{\sim}{\Lambda}$	Diagonal matrix containing eigenvalues Λ_k of $\underset{\sim}{\Phi}(T,0)$
V	Velocity of forward flight of the whole rotor	μ	Advance ratio
w_e, w_{eo}	Elastic part of the displacement of a point on the elastic axis of the blade, in the k direction, approximately, (Fig. 1)	μ_C	Critical value of advance ratio at which flap-lag system becomes unstable
		ρ_A	Density of air
x,y,z	Rotating orthogonal coordinate system	σ	Blade solidity ratio
$x_o = x - e_1$	Running spanwise coordinate for part of the blade free to deflect elastically	$\Phi(\psi, \psi_o)$	State transition matrix at ψ, for initial conditions given at ψ_o
X_H, Y_G	Defined in Appendix B	ψ	Azimuth angle of blade ($\psi = \Omega t$) measured from straight aft position
α	Angle of reversed flow region (Fig. 2)		
α_R	Angle of attack of the whole rotor	ω_C	Flutter frequency
		ω_k	Imaginary part of kth characteristic exponent

$\overline{\omega}_{F1}, \overline{\omega}_{L1}$ Natural frequency of ith flap or lag mode, rotating

Ω Speed of rotation

Special Symbols

$(\overline{})$ Nondimensionalized quantity, length for elastic properties nondimensionalized w.r.t. ℓ; all other w.r.t. R frequencies w.r.t. Ω; mass properties w.r.t. I_b

$()'$ Differentiation w.r.t. $\overline{x}_o$

$(\overset{*}{})$ Differentiation w.r.t. ψ

$()_R, ()_I$ Subscripts, denoting real and imaginary parts of the appropriate quantity

$\underset{\sim}{()}$ The symbol beneath a quantity denotes a vector or a matrix

$\underset{\sim}{()}^{-1}$ Denotes the inverse of a matrix

The dynamics of a helicopter blade in forward flight are usually described by a system of linear differential equations with periodic coefficients. A growing acceptance of hingeless helicopter blades for conventional helicopters flying at relatively high forward flight speeds has intensified the need for fundamental research on the aeroelastic stability of such systems.

Studies dealing with the effect of forward flight (or periodic coefficients) have been primarily devoted to the study of flapping instability at high advance ratios.[1-8] A limited number of studies dealing with the effect of periodic coefficients on coupled flap-lag[9,10] or coupled flap-lag-pitch[11] motion were also conducted. The case of coupled flap-lag motion has been, somewhat inconclusively, investigated by Hall[10] using multivariable Floquet theory, the same problem was also considered by Friedmann and Tong[9] but the treatment was limited to low advance ratios ($\mu < 0.3$). The coupled, linearized, flap-lag-torsion motion has been investigated by Crimi[11] using a modified Hill method. In both cases[10,11] only a limited number of numerical results were obtained and the physical mechanism of the aeroelastic instabilities has not been clearly identified, in particular the degree of freedom which triggers the instability was not identified and the results for forward flight were not compared with those for hover.

Recent investigation of the aeroelastic stability of hingeless blades in hover[12] indicated that the aeroelastic stability boundaries are quite sensitive to the number of degrees of freedom employed in the analysis. Therefore it is important to determine how the flapping behavior of a blade at high advance ratios is modified by the lag degree of freedom. This important problem, which has not received adequate treatment before, is one of the main topics of the present study.

The mathematical methods used in previous studies dealing with the effects of forward flight were: (a) The rectangular ripple method[1], (b) Analog computer simulation,[3,4] (c) Various forms of Hill's method,[2,11] (d) Multivariable Floquet-Liapunov theory,[6,7,10] (e) Perturbation method in multiple time scales.[8,9] The mathematical method employed in the present study is the Floquet-Liapunov theorem, and the transition matrix is evaluated by two separate methods. It is also shown that careful use of this method enables one to circumvent problems associated with identifying the results encountered in previous studies.[10]

In addition, a new and convenient approximation for the reversed flow region is developed, this approximation is believed to be adequate for most blade stability analyses. Finally, the effects of various important parameters such as collective pitch setting, structural damping, droop and preconing on the instability associated with forward flight is investigated.

1. The Equations of Motion

1.1 Basic Assumptions

The present study is based upon a consistently derived system of equations of motion for the linearized coupled flap-lag motion of a cantilevered rotor blade at arbitrary advance ratios.

The derivation itself is algebraically tedious, thus only a brief outline will be given in this paper, the complete details of the derivation can be found elsewhere.[13]

The geometry of the problem is shown in Fig. 1. The following basic assumptions were used in deriving the equations of motion: (a) The blade is cantilevered at the hub. It can have an angle of droop β_D at the root. In addition, the feathering axis can be preconed by an angle β_P. The angles β_D and β_P are small. (b) The blade can bend in two directions normal to the elastic axis and is torsionally rigid. (c) The deflections of the blade are moderately small so that terms of $O(\varepsilon_D^2)$ can be neglected compared to one. (d) Moderately large deflections have only a small effect on the tension due to elastic effects on the blade since one of its ends is free, thus a linear treatment of the elastic restoring forces is adequate. (e) Two dimensional quasi-steady aerodynamic strip theory is used $C(k)=1$ and apparent mass effects are neglected. (f) Reversed flow is included using an approximate model for reversed flow described in Appendix C. (g) Stall and compressibility effects are neglected.

Using the assumptions given above a system of nonlinear partial differential equations for the coupled flap-lag motion of the blade is derived, with respect to an x,y, and z coordinate system rotating with the blade. The derivation follows essentially along the lines of Reference 14, all the details can be found in Reference 13.

1.2 Brief Derivation of the Equations of Motion

The differential equation for the dynamic stability of a cantilevered rotor blade can be written as

$$\frac{\partial^2}{\partial x_o^2}\left\{[(EI)_y + E_{C1}]\frac{\partial^2 w_e}{\partial x_o^2} + E_{C2}\frac{\partial^2 v_e}{\partial x_o^2}\right\} - \frac{\partial}{\partial x_o}[T\frac{\partial w}{\partial x_o}] = P_z$$

$$\frac{\partial^2}{\partial x_o^2}\left\{[(EI)_z - E_{C1}]\frac{\partial^2 v_e}{\partial x_o^2} + E_{C2}\frac{\partial^2 w_e}{\partial x_o^2}\right\} - \frac{\partial}{\partial x_o}[T\frac{\partial v}{\partial x_o}] = P_y$$

$$(1)$$

where the quantities E_{C1}, E_{C2} are given in Appendix A.

The distributed loading terms in the x,y and z directions with terms up to $O(\epsilon_D^3)$ in displacements can be written as

$$P_x = \frac{T}{x_o} = m\Omega^2[(x_o + e_1) + 2\overset{*}{v}]$$

$$P_y = L_y - m\Omega^2[\overset{**}{v} - (e_o + v) + 2\overset{*}{u}] - g_{SL}\Omega\overset{*}{v}$$

$$P_z = L_z - m\Omega^2\overset{**}{w} - g_{SF}\Omega\overset{*}{w} \qquad (2)$$

The boundary conditions for this kind of blade are well known.[14] The displacement field of the blade with $\sin\theta \cong \theta$ and $\cos\theta \cong 1$ can be written as[13,14]

$$u = -w_e(\beta_P + \beta_D) - \frac{x_o}{2}(\beta_P + \beta_D)^2 - \frac{1}{2}\int_o^{x_o}\left[\left(\frac{\partial v_e}{\partial x_1}\right)^2 + \left(\frac{\partial w_e}{\partial x_1}\right)^2\right]dx_1$$

$$v = v_e - x_o\beta_D\theta$$

$$w = w_e + x_o(\beta_P + \beta_D) \qquad (3)$$

and

$$w_e = \sum_{k=1}^{N}\ell\,\eta_k(x_o)g_k(t) = \ell\,\eta_k g_k$$

$$v_e = -\sum_{m=1}^{M}\ell\,\gamma_m(x_o)h_m(t) = -\ell\,\gamma_m h_m \qquad (4)$$

where it is understood that repeated indices imply summation unless otherwise stated.

The aerodynamic loads L_z and L_y are given by[13,14]

$$L_z = a\rho_A bR\,U_T(U_T\theta - U_P) \qquad (5)$$

$$L_y = a\rho_A bR\left[U_P(U_T\theta - U_P) + \frac{C_{do}}{a}U_T^2\right] \qquad (6)$$

where the velocities U_P and U_T are given by

$$U_P = \Omega\overset{*}{w} + \Omega R\left(\lambda + \mu\cos\psi\,\frac{\partial w}{\partial x_o}\right) \qquad (7)$$

$$U_T = \Omega\overset{*}{v} + \Omega R\left(\overline{x} + \mu\sin\psi + \mu\cos\psi\,\frac{\partial v}{\partial x_o}\right) \qquad (8)$$

The last term in Equation (8) is due to the radial flow along the blade. This term has been neglected in some previous analyses. For arbitrary advance ratios this is an important and non-negligible term.

Combination of Equations (1) through (8) and application of Galerkin's method to eliminate the spatial variable reduces the problem to a system of ordinary differential equations.

$$M_{Fi}\overset{**}{g}_i + 2\,\overline{\omega}_{Fi}\overline{M}_{Fi}\eta_{SFi}\overset{*}{g}_i + \overline{E}^S_{1k}g_k + \overline{\omega}^2_{Fi}M_{Fi}g_i = \overline{E}^{cs}_{im}h_m$$

$$+ 2\,\overline{P}_{ikm}\overset{*}{g}_k h_m - (\beta_D + \beta_P)\overline{B}^1_i + 2(\beta_P + \beta_D)\overline{B}^3_{im}h_m + A_{Fi} \qquad (9)$$

$$\overline{M}_{Li}\overset{**}{h}_i + 2\,\overline{M}_{Li}\overline{\omega}_{Li}\eta_{SLi}\overset{*}{h}_i + \overline{M}_{Li}\overline{\omega}^2_{Li}h_i - \overline{E}^S_{im}h_m = \overline{E}^{cs}_{ik}g_k$$

$$- 2\,\overline{B}^7_{ik}(\beta_P + \beta_D)\overset{*}{g}_k + \overline{B}^{11}_i\beta_D\theta + 2[\overline{S}_{imr} - (\overline{M}_\gamma)_{imr}]\overset{*}{h}_m h_r$$

$$- 2(\overline{M}_\eta)_{ik\ell}\overset{*}{g}_k g_\ell - \overline{B}^{10}_i\beta_D\theta + 2\,\overline{B}^8_{im}\beta_D\theta\overset{*}{h}_m + A_{Li} \qquad (10)$$

where the various quantities $\overline{M}_{Fi}$, $\overline{P}_{1km}$, $\overline{M}_{Li}$, $\overline{S}_{imr}$, $(\overline{M}_\eta)_{ik\ell}$ are generalized mass integrals given in References 13 and 14, and also in Reference 12 (for $i = k = \ell = m = r = 1$). While the quantities $\overline{B}^1_i$, $\overline{B}^3_{1m}$, $\overline{E}^S_{1k}$, $\overline{E}^{cs}_{im}$, $\overline{E}^S_{im}$, $\overline{E}^{cs}_{ik}$, $\overline{B}^{11}_i$, $\overline{B}^7_{1k}$, $\overline{B}^{10}_i$ amd $\overline{B}^8_{im}$ etc. are given in Appendix A. The quantities A_{Fi}, A_{Li} are generalized aerodynamic forces defined by

$$A_{Fi} = \ell^2\int_{\overline{A}}^{\overline{B}}L_z\,\eta_i d\overline{x}_o/\Omega^2 I_b \qquad (11)$$

$$A_{Li} = \ell^2\int_{\overline{A}}^{\overline{B}}L_y\,\gamma_i d\overline{x}_o/\Omega^2 I_b \qquad (12)$$

Equations (9) and (10) are coupled nonlinear ordinary differential equations. In the present study these equations will be linearized about a suitable equilibrium position, which is taken to be the steady state equilibrium position of the blade in <u>hover</u>. Through this process of linearization many nonlinear terms are transformed into coupling terms. At this stage one encounters a considerable number of terms which are small and therefore negligible. In order to neglect the appropriate terms a rational ordering scheme is used which enables one to neglect terms in a systematic manner. In this scheme all the important parameters of the problem are assigned orders of magnitudes in terms of a typical displacement quantity ϵ_D thus:

$$\frac{v}{R} = 0(\epsilon_D); \quad \frac{w}{R} = 0(\epsilon_D); \quad \overline{x} = 0(1); \quad \mu = 0(1);$$

$$\lambda = 0(\epsilon_D); \quad \theta = 0(\epsilon_D)$$

$$\frac{\partial w}{\partial x_o} = 0(\epsilon_D); \quad \frac{\partial v}{\partial x_o} = 0(\epsilon_D); \quad \beta_D = \beta_P = 0(\epsilon_D);$$

$$\frac{C_{do}}{a} = 0(\epsilon_D^2) \qquad (13)$$

An order of magnitude analysis of the equations indicates that in general terms up to and including $0(\epsilon_D^2)$ must be included in the linearized flap equations, while for lag equations some $0(\epsilon_D^3)$ terms have to be retained.

The process of the linearization consists of expressing the elastic part of the displacement field as

58

$$w_e = w_{eo} + \Delta w_e = \eta_k (g_k^o + \Delta g_k)$$

$$v_e = v_{eo} + \Delta v_e = -\gamma_m (h_m^o + \Delta h_m) \qquad (14)$$

where the static equilibrium condition in hover is given by

$$\bar{E}_{ik}^s g_k^o + \bar{\omega}_{Fi}^2 M_{Fi} g_i^o - \bar{E}_{im}^{cs} h_m^o = -(\beta_P + \beta_D) \bar{B}_i^1 + \frac{\gamma}{2} (\frac{\ell}{R})^2 (\theta F_i^1 - \lambda F_i^2)$$

where $i = 1, 2, \ldots, N$

$$- \bar{E}_{ik}^{cs} g_k^o + \bar{M}_{Li} \bar{\omega}_{Li}^2 h_i^o - \bar{E}_{im}^s h_m^o = \beta_D \theta (\bar{B}^{11} - \bar{B}^{10})$$

$$+ \frac{\gamma}{2} (\frac{\ell}{R})^2 [\lambda (\theta L_i^1 - \lambda L_i^2) + \frac{C_{do}}{a} L_i^4] \quad i = 1, 2, \ldots M \qquad (15)$$

The various quantities F^1, L^1 are defined in Appendix A. Next, for the sake of simplicity, the equations are specialized to the case of one elastic mode for each degree of freedom, i.e. one flapping and one lead-lag mode.

Furthermore for mathematical convenience the equations of motion have to be transformed into a system of first order equations. This is achieved by using the following notation

$$\overset{*}{\Delta g_1} = y_1 \quad ; \quad \overset{*}{\Delta h_1} = y_3$$
$$\Delta g_1 = y_2 \quad ; \quad \Delta h_1 = y_4 \qquad (16)$$

For the stability analysis, only the homogeneous part of the equations of motion is required, thus the equations of motion in their final form can be written as

$$\overset{*}{y} = A(\psi) y \qquad (17)$$

where A is a 4x4 matrix defined in Appendix B.

The equations of motion (17) will have a different form for the normal flow region and for the reversed flow region. The representation of the reversed flow together with its effect on the form of Equations (17) is described in Appendix C.

2. Method of Solution

The stability investigation of the blade motions is based upon the Floquet-Liapunov theorem[15] which states the knowledge of the state transition matrix over one period is sufficient in order to determine the stability of a periodic system having a common period T. Based upon the Floquet-Liapunov theorem, the transition matrix for the periodic system can be written as[15]

$$\Phi(\psi, \psi_o) = P^{-1}(\psi) e^{R(\psi - \psi_o)} P(\psi_o) \qquad (18)$$

where

$$P(\psi + T) = P(\psi) \qquad (19)$$

where R is a constant matrix and $P(t)$ is a periodic matrix. Clearly the stability of the system is determined by the matrix R, where R is given by following relation

$$\Phi(T, 0) = e^{RT} = C \qquad (20)$$

A direct result of the Floquet-Liapunov theorem is that the knowledge of the transition matrix over one period determines the solution to the homogeneous system everywhere through the relation

$$\Phi(\psi + sT, 0) = \Phi(\psi, 0) (e^{RT})^s \qquad (21)$$

where $0 \leq \psi \leq T$, s any integer.

In general R is a fully populated (nxn) square matrix. If it has n independent eigenvalues, it is well known from elementary linear algebra[15] that a similarity transformation can be found such that

$$Q^{-1} R Q = \lambda \qquad (22)$$

where the columns of Q are the n-linearly independent eigenvectors of R and λ is a diagonal matrix whose elements are the eigenvalues of R. Combining Equations (20) and (22) and using the definition of the matrix exponential[15] one has

$$e^{RT} = Q e^{\lambda T} Q^{-1} = C$$

or

$$e^{\lambda T} = \Lambda = Q^{-1} C Q = Q^{-1} \Phi(T, 0) Q \qquad (23)$$

where Λ is a diagonal matrix containing the eigenvalues of the transition matrix at the end of one period. The eigenvalues of $\Phi(T, 0)$ or the characteristic multipliers are related to the eigenvalues of R, denoted characteristic exponents, through the relation

$$e^{\lambda_k T} = \Lambda_k \qquad k = 1, 2, \ldots r \qquad (24)$$

Clearly λ_k and Λ_k are both complex quantities in general, thus

$$\lambda_k = \zeta_k + i \omega_k$$
$$\Lambda_k = \Lambda_{kR} + i \Lambda_{kI} \qquad (25)$$

from which

$$\zeta_k = \frac{1}{2T} \ln[\Lambda_{kR}^2 + \Lambda_{kI}^2] \qquad (26)$$

and

$$\omega_k = \frac{1}{T} \tan^{-1} \frac{\Lambda_{kI}}{\Lambda_{kR}} \qquad (27)$$

the quantity ω_k can be determined according to the Floquet-Liapunov theory only within an integer multiple of the nondimensional period.

The stability criteria for the system is related to the eigenvalues of R or the real part of the characteristic exponents ζ_k. The solutions of the Equation (17) approach zero as $\psi \to \infty$ if

$$|\Lambda_{kR}^2 + \Lambda_{kI}^2| < 1 \quad \text{or} \quad \zeta_k < 0 \quad k = 1, 2, \ldots, n$$

Finally a brief description of the numerical implementation of the scheme described above will be given. The transition matrix at the end of one period $\Phi(T,0)$ is evaluated using direct numerical integration. Equations (17) are integrated for the set of initial conditions corresponding to $\Phi(0,0) = I$. The numerical integration is performed using a fourth order Runge Kutta method. The eigenvalues of the transition matrix are evaluated by a Jacobi type eigenvalue routine. For some of the cases the value of $\Phi(T,0)$ has been evaluated using Hsu's method.[13,17] This was done in order to obtain results by two different numerical schemes and also because Hsu's method was found to be more efficient numerically. Both methods yield identical results, therefore it is not specified on the plots which scheme was used to evaluate $\Phi(T,0)$.

3. Results and Discussion

3.1 Numerical Quantities Used in the Calculations

In computing the numerical results the following assumptions were made,

Mass and stiffness distribution was assumed to be constant along the span of the blade. Two different kinds of mode shapes were used:

(a) For most of the cases for which essentially trend type studies were conducted an assumed mode shape in flap and lap was used as given by the appropriate expression in Reference 12. When an assumed mode shape is used the elastic coupling effect[16] is neglected.

(b) For a few cases an exact rotating mode shape in flap and lag was employed. These mode shapes were generated by using Galerkin's method based upon five nonrotating cantilever mode shapes for each flap or lag degree of freedom. For these cases the elastic coupling effect was included.

The coefficients F^i, L^i and $\bar{B}^i$ defined in Appendix A and in References 12 through 14 were evaluated using seven point Gaussian integration. For the region of reversed flow these coefficients were treated in a special manner as explained in Appendix C.

For the cases computed the inflow was evaluated using an expression for constant inflow ratio in <u>hover</u>, given by

$$\lambda = \frac{a\sigma}{16} \left[\sqrt{1 + \frac{24\theta}{a\sigma}} - 1 \right] \qquad (28)$$

This inflow relation is equivalent to taking the induced velocity of 3/4 blade radius as representative of a constant induced velocity over the whole disk. It is clear that for forward flight one should use the expression

$$\lambda = \mu \tan\alpha_R + C_T/2 \sqrt{\mu^2 + \lambda^2} \qquad (29)$$

Use of this relation would have required the use of a trim procedure in the calculations. It

can be seen from Reference 14 that the requirement of trimmed flight at a fixed C_T results in an increase of θ at advance ratios of $\mu > .3$ and it also requires continuous changes in θ_{1c}^* and θ_{1s}. The experience gained when using this approach in Reference 14 indicates that when the trim requirement is included in the calculation, the value of μ_c at which instability will occur will be usually lower. Furthermore, when using this approach it was found that it is difficult to determine which part of the degradation in stability is related to the increase in θ, θ_{1s} and θ_{1c} and which part is due to the periodic coefficients. This added complication is not warranted in a trend study such as the present one, and it is not consistent with the stated purpose of this paper, which is; a clear illustration of the effects of the periodic coefficients when the lag degree of freedom is included in the formulation of the problem.

Finally, in all the computations the following values were used:

$$C_{do} = .01; \quad a = 2\pi; \quad \sigma = .05; \quad e_1 = 0; \quad \bar{A} = 0. \; ; \quad \bar{B} = 1$$

Various other pertinent quantities are specified on the plots.

3.2 Results

The results obtained in the present study usually are given in form of plots representing the variation of the real part of the characteristic exponent ζ_k with the advance ratio μ. Most of the cases presented in this study were evaluated using an assumed mode shape, as described in the previous section, and neglecting the elastic coupling effect.

For some cases an exact rotating mode shape in flap and lead-lag was used and the elastic coupling was included, when this approach was used a statement to this effect appears on the appropriate plots. When no such statement appears it is to be understood that the assumed mode shape is used and the elastic coupling is neglected.

A typical case is shown in Figure 3 for a collective pitch setting of $\theta = .15$. Starting the computation at $\mu = 0$, enables one to easily identify the instabilities encountered, by using results previously obtained for hover. As shown the lag degree becomes unstable and the frequency of the oscillation is $\omega_k = 1.28119$. This result clearly indicates that by neglecting the lag degree of freedom one could obtain completely incorrect stability boundaries.

The importance of the reversed flow region is illustrated by Figure 4. As shown with the reversed flow region the instability occurs at higher values of μ than without the reversed flow region. Similar trends were observed in previous studies when only the flapping motion was considered,[5] indicating that by neglecting the reversed flow region one could expect conservative results from a stability point of view. It also

$^*\theta_{1c}, \theta_{1s}$ cyclic pitch changes.

indicates that in this particular case the reversed flow region starts being important above advance ratios of $\mu = 0.8$.

It is important to note that the frequency at which the lag degree of freedom becomes unstable is not 1/2 or 1 as is usual for the case of parametric excitation. Thus it seemed important to identify the source of this destabilizing effect. The results of this study are presented in Figures 5 and 6. The effect of neglecting the radial flow terms on the real part of the characteristic exponent, associated with the flap degree of freedom, is shown in Figure 5. As shown, the radial flow terms have a stabilizing effect on the flapping motion with the radial flow forms suppressed the flap degree of freedom becomes unstable at $\mu=1.33$. The effect of the radial flow terms on the lead-lag degree of freedom is illustrated by Figure 6, as shown without the radial flow terms the instability in the lag degree of freedom is completely eliminated and the system becomes unstable in flap. When the radial flow terms are included, the lag degree of freedom is the critical one and the system becomes unstable at $\mu=.754$. This matter was pursued further by identifying the actual destabilizing term in the equations of motion, which was found to be an aerodynamic coupling term. This term couples the flap motion with the lag motion in the flap equation, its form is

$$ \mu^2 \cos^2\psi \, \frac{\partial w}{\partial x_o} \, \frac{\partial u}{\partial x_o} $$

This term is due to the $U_T U_P$ term in Equation (5). The term shown above is the complete nonlinear one, clearly the one retained in the equations of motion is the coupling term obtained from linearizing this expression.

As mentioned in the previous section the results presented in Figures 3 through 6 were obtained by neglecting the elastic coupling effect. In order to asses the effect of this assumption the typical case has been also recomputed with the exact mode shape and the elastic coupling effect, the results are shown in Figure 11. From Figure 11 it is clear that use of the exact rotating mode in flap and lag reduces the value of μ_c to $\mu_c = 0.653$, when the elastic coupling is also included μ_c is further reduced to $\mu_c = .583$. Thus, for this case, μ_c seems to be more sensitive to the type of mode shape used than to the inclusion of the elastic coupling effect. It is also interesting to note, that for this case the elastic coupling effect is destabilizing, while for hover its effect on θ_c is quite stabilizing.

Previous studies[12] dealing with the effect of viscous type of structural damping on the stability boundaries for hover indicated that this parameter has an important stabilizing. The effect of this parameter for forward flight is shown by Figures 7 and 8. The stabilizing effect of structural damping in the lag degree of freedom is evident from Figure 7, where the real part of the characteristic exponent associated with the

lead-lag degree of freedom is plotted as a function of the advance ratio μ, again only the structural damping in lag is important. A summary of these results is presented in Figure 8 showing the variation of μ_c as a function of the structural damping. It is interesting to note that this plot indicates that the greatest stabilizing effect due to structural damping is obtained in the range $0 < \eta_{SL1} < .02$ (2% of critical damping), after which, the gain in stability tends to level off. Similar trends were obtained from stability studies in hover.[12]

Again in order to illustrate the sensitivity of the results to the mode shape and elastic coupling, the results have been recomputed with these effects included; these results are also shown in Figure 8. As seen the use of the correct mode shape and the elastic coupling effect reduce the value of μ_c, at which instability occurs.

The sensitivity of the results, to different collective pitch settings is illustrated by Figure 9. Comparison of Figures 3 and 9 indicates that by decreasing the collective pitch setting from $\theta = .15$ to $\theta = .05$ eliminated the instability associated with the lead-lag motion. The instability in this case occurs at $\mu_c = 1.88$ with a frequency of 0 or 1. This is a typical flapping instability due to the periodic coefficients. Comparison of Figures 3 and 9 seems to indicate that the assumption of nonlifting rotors used in some forward flight studies[7] can be nonconservative.

Finally, Figure 10 shows the dependence of μ_c on the angle of droop β_D. As shown μ_c is relatively insensitive to β_D. On the other hand β_D has a very important effect on the value of θ_c at which the linearized system in hover becomes unstable.

It should be also noted that a considerable number of additional numerical results, including the effects of elastic coupling can be found in Reference 13.

4. Conclusions

The major conclusions obtained from the present study are summarized below. They should be considered indicative of trends and their application to the design of a helicopter blade should be limited by the assumptions used.

(1) Flapping instability and response studies at high advance ratios can be inaccurate and misleading due to the neglection of the lag degree of freedom. The effect of the periodic coefficients on the coupled flap-lag system shows that in general instability can occur at lower values of advance ratios than when the flap degree of freedom is considered by itself.

(2) In addition to the instabilities associated with the periodic coefficients (i.e. with frequencies of 0, 1 or 1/2) the coupled flap-lag

61

system has the tendency to become unstable due to an aerodynamic coupling effect associated with the radial flow terms. This instability which has a frequency close to the rotating lag frequency of the system, occurs usually at values of μ_c much lower than those for which the flapping degree of freedom becomes unstable.

(3) Viscous type of structural damping in the lead-lag degree of freedom has a stabilizing effect on the instability discussed in previous conclusion.

(4) The value of the collective pitch setting has a considerable effect on the value of the advance ratio at which instabilities due to the periodic coefficients or the radial flow aerodynamic coupling terms occur. Increase in collective pitch is destabilizing, therefore high advance ratio studies which do not include this effect (nonlifting rotors) may yield nonconservative results.

(5) The numerical results obtained in the present study agree with the analytical results obtained previously[9] indicating that hingeless blades with a rotating lag stiffness of 1/2 or 1 can easily become unstable due to the effect of periodic coefficients.

(6) While droop has a very strong effect on the stability boundaries of hingeless blades in hover, it has a very minor effect on the stability boundary in forward flight.

References

1. Horvay, G. and Yuan, S.W., STATILITY OF ROTOR BLADE FLAPPING MOTION WHEN THE HINGES ARE TILTED. GENERALIZATION OF THE 'RECTANGULAR RIPPLE' METHOD OF SOLUTION, Journal of the Aeronautical Sciences, October 1947, pp. 583-593.

2. Shulman, Y., STABILITY OF A FLEXIBLE HELICOPTER ROTOR BLADE IN FORWARD FLIGHT, Journal of the Aeronautical Sciences, July 1956, pp. 663-670, 693.

3. Sissingh, G.J., DYNAMICS OF ROTOR OPERATING AT HIGH ADVANCE RATIOS, Journal of American Helicopter Society, July 1968, pp. 56-63.

4. Sissingh, G.J., and Kuczynski, W.A., INVESTIGATIONS ON THE EFFECT OF BLADE TORSION ON THE DYNAMICS OF THE FLAPPING MOTION, Journal of the American Helicopter Society, April 1970, pp. 2-9.

5. R & M No. 3544, THE STABILITY OF ROTOR BLADE FLAPPING MOTION AT HIGH TIP SPEED RATIOS, Lowis, O.J., 1968.

6. Peters, D.A., and Hohenemser, K.H., APPLICATION OF THE FLOQUET TRANSITION MATRIX TO PROBLEMS OF LIFTING ROTOR STABILITY, Journal of the American Helicopter Society, April 1971, pp. 25-33.

7. Hohenemser, K.H., and Yin, S.K., SOME APPLICATIONS OF THE METHOD OF MULTIBLADE COORDINATES, Journal of American Helicopter Society, July 1972, pp. 3-12.

8. Johnson, W., A PERTURBATION SOLUTION OF ROTOR FLAPPING STABILITY, AIAA Paper 72-955.

9. Friedmann, P. and Tong, P., NONLINEAR FLAP-LAG DYNAMICS OF HINGELESS HELICOPTER BLADES IN HOVER AND IN FORWARD FLIGHT, Journal of Sound and Vibration, September 1973.

10. SUDAAR No. 400, APPLICATION OF FLOQUET THEORY TO THE ANALYSIS OF ROTARY WING VTOL STABILITY, HALL, W.E., Stanford University, February 1970.

11. NASA CR-1332, A METHOD FOR ANALYZING THE AEROELASTIC STABILITY OF A HELICOPTER ROTOR IN FORWARD FLIGHT, Crimi, P., August 1969.

12. Friedmann, P., AEROELASTIC INSTABILITIES OF HINGELESS HELICOPTER BLADES, AIAA Paper 73-193 January 1973, (also Journal of Aircraft, October 1973).

13. UCLA School of Engineering and Applied Science Report, AEROELASTIC STABILITY OF COUPLED FLAP-LAG MOTION OF HELICOPTER BLADES AT ARBITRARY ADVANCE RATIOS, Friedmann, P., and Silverthorn, J.L., to be published January 1974.

14. NASA-CR-114 485, DYNAMIC NONLINEAR ELASTIC STABILITY OF HELICOPTER ROTOR BLADES IN HOVER AND FORWARD FLIGHT, Friedmann, P., and Tong, P., May 1972.

15. Brockett, R.W., FINITE DIMENSIONAL LINEAR SYSTEMS, John Wiley and Sons, 1970.

16. Ormiston, R.A., and Hodges, D.H., LINEAR FLAP-LAG DYNAMICS OF HINGELESS HELICOPTER ROTOR BLADES IN HOVER, Journal of the American Helicopter Society, Vol. 17, No. 2, April 1972, pp. 2-14.

17. Hsu, C.S., and Cheng, W.H., APPLICATION OF THE THEORY OF IMPULSIVE PARAMETRIC EXCITATION AND NEW TREATMENTS OF GENERAL PARAMETRIC EXCITATION PROBLEMS, Journal of Applied Mechanics, March 1973, pp. 78-86.

Appendix A. Definitions of the Generalized Masses, Aerodynamic Integrals and other Quantities

The quantities, $\overline{P}_{111}, \overline{M}_{F1}, \overline{M}_{L1}, \overline{S}_{111}, (\overline{M}_\eta)_{111}, (\overline{M}_\gamma)_{111}$ are generalized masses given, in Appendix A of Reference 12, with the general i,m,k indices these quantities can be found in References 13 and 14.

$$\bar{B}_1^1 = \ell^3 \int_0^1 \left[\int_{\bar{x}_1}^1 m(\bar{x}_1 + \bar{e}_1) d\bar{x}_1 \right] \eta_i' \, d\bar{x}_0 / I_b$$

$$\bar{B}_{im}^3 = \ell^3 \int_0^1 \eta_i' \left[\int_{\bar{x}_0}^1 m \gamma_m d\bar{x}_1 \right] d\bar{x}_0 / I_b$$

$$\bar{B}_{im}^7 = \ell^3 \int_0^1 m \eta_i \gamma_m d\bar{x}_0 / I_b ;$$

$$\bar{B}_{im}^8 = \ell^3 \int_0^1 \left[\int_{\bar{x}_0}^1 m \gamma_m d\bar{x}_1 \right] d\bar{x}_0 / I_b$$

$$\bar{B}_{im}^{10} = \ell^3 \int_0^1 \gamma_i \left[\int_{\bar{x}_0}^1 m(\bar{x}_1 + \bar{e}_1) d\bar{x} \right] d\bar{x}_0 / I_b ;$$

$$\bar{B}_1^{11} = \ell^3 \int_0^1 \bar{x}_0 m \gamma_i \, d\bar{x}_0 / I_b$$

$$I_b = \ell^3 \int_0^1 m \bar{x}_0^2 \, d\bar{x}_0$$

Structural damping is represented by

$$g_{SF} = 2 \, \Omega \, \bar{\omega}_{Fi} \, \eta_{SF_i} \quad ; \quad g_{SL} = 2 \, \Omega \, \bar{\omega}_{Li} \, \eta_{SL_i}$$

The elastic coupling effect is represented by

$$E_{C1} = [(EI)_z - (EI)_y] \sin^2\theta; \quad E_{C2} = [(EI)_z - (EI)_y] \sin\theta\cos\theta$$

$$\int_0^1 E_{C1} \eta_k'' \eta_i'' \, d\bar{x}_0 = \bar{E}_{ik}^s \, I_b \Omega^2 \ell$$

$$\int_0^1 E_{C2} \gamma_m'' \eta_i'' \, d\bar{x}_0 = \bar{E}_{im}^{cs} \, I_b \Omega^2 \ell$$

$$\int_0^1 \gamma_i'' \gamma_m'' E_{C1} d\bar{x}_0 = \bar{\bar{E}}_{im}^s \, I_b \Omega^2 \ell$$

$$\int_0^1 \gamma_i'' \eta_k'' E_{C2} d\bar{x}_0 = \bar{\bar{E}}_{ik}^{cs} \, I_b \Omega^2 \ell$$

When using these expressions in a one mode analysis for each degree of freedom the lower indices are deleted for these expressions and the expressions for the generalized aerodynamic integrals. The generalized aerodynamic integrals F^1, L^1 can be found in References 12,13 and 14. For this study some additional expressions had to be defined, only these are given below.

$$F_{1m}^{21} = \int_{\bar{A}}^{\bar{B}} \bar{x}_0 \eta_i \gamma_m' d\bar{x}_0 ; \quad F_{1m}^{22} = \int_{\bar{A}}^{\bar{B}} \eta_i \gamma_m' \, d\bar{x}_0$$

$$F_{1km}^{23} = \int_{\bar{A}}^{\bar{B}} \eta_i \eta_k' \gamma_m' d\bar{x}_0 ; \quad F_{1km}^{24} = \int_{\bar{A}}^{\bar{B}} \eta_i \eta_k \gamma_m' d\bar{x}_0$$

$$L_{1m}^{20} = \int_{\bar{A}}^{\bar{B}} \gamma_i \gamma_m' d\bar{x}_0 ; \quad L_{1km}^{21} = \int_{\bar{A}}^{\bar{B}} \gamma_i \eta_k' \gamma_m' d\bar{x}_0$$

$$L_{1km}^{22} = \int_{\bar{A}}^{\bar{B}} \gamma_i \eta_k \gamma_m' d\bar{x}_0 ; \quad L_{1m}^{23} = \int_{\bar{A}}^{\bar{B}} \gamma_i \gamma_m' \bar{x} \, d\bar{x}_0$$

$$L_{1k\ell}^{24} = \int_{\bar{A}}^{\bar{B}} \gamma_i \eta_k' \eta' \, d\bar{x}_0$$

Appendix B. Elements of the A - Matrix

The elements of the $\underset{\sim}{A}$ - matrix, which defines the equations of motion when written as first order differential equations, are given below:

$$A_{21} = 1; \quad A_{22} = A_{23} = A_{24} = 0$$

$$A_{43} = 1; \quad A_{41} = A_{42} = A_{44} = 0$$

$$A_{11} = -\bar{g}_{D1} + \frac{\gamma}{2} \left(\frac{\ell}{R} \right)^3 \mu(-F^9 \sin\psi + F^{24} h_1^o \cos\psi)$$

$$A_{12} = -\left(\bar{\omega}_{F1}^2 + \frac{\bar{E}^s}{\bar{M}_{F1}} \right) + \frac{\gamma}{2} \left(\frac{\ell}{R} \right)^2 \left[-\left(\frac{\mu^2}{2} F^7 \sin 2\psi + \mu F^6 \cos\psi \right) \right.$$
$$\left. + \frac{\mu^2}{2} F^{23} h_1^o (1+\cos 2\psi) \right]$$

$$A_{13} = X_H + \frac{\gamma}{2} \left(\frac{\ell}{R} \right)^3 \left[-2\theta\mu F^{11} \sin\psi + \mu(\beta_p + \beta_D) F^{11} \cos\psi \right.$$
$$\left. + F^{14} g_1^o \mu \cos\psi \right]$$

$$A_{14} = \frac{\bar{E}^{cs}}{\bar{M}_{F1}} + \frac{\gamma}{2} \left(\frac{\ell}{R} \right)^2 \left\{ \theta(-2F^{21}\mu\cos\psi - \mu^2 \sin 2\psi F^{22}) \right.$$
$$\left. + \lambda\mu F^{22} \cos\psi + \frac{\mu^2}{2}(1+\cos 2\psi)[F^{23}g_1^o + F^{22}(\beta_p + \beta_D)] \right\}$$

$$A_{31} = Y_G + \frac{\gamma}{2} \left(\frac{\ell}{R} \right)^3 [\theta L^8 \mu \sin\psi - 2\mu L^{17} g_1^o \cos\psi - \theta\mu L^{22} h_1^o \cos\psi$$
$$- 2\mu(\beta_p + \beta_D)L^8 \cos\psi]$$

$$A_{32} = \frac{\bar{\bar{E}}_{cs}}{\bar{M}_{L1}} + \frac{\gamma}{2} \left(\frac{\ell}{R} \right)^2 \left[\theta(\frac{\mu^2}{2} L^{11} \sin 2\psi + L^{10} \mu \cos\psi) \right.$$
$$- 2\lambda L^{11}\mu \cos\psi - \theta\frac{\mu^2}{2}(1+\cos 2\psi)L^{21}h_1^o -$$
$$- \mu^2(\beta_p + \beta_D)L^{11}(1+\cos 2\psi) - L^{24}\mu^2 g_1^o (1+\cos 2\psi) \Big]$$

$$A_{33} = -\bar{g}_{D2} + \frac{\gamma}{2} \left(\frac{\ell}{R} \right)^3 [-\theta\mu L^{16} g_1^o \cos\psi - 2 \frac{C_{Do}}{a} \mu L^{13} \sin\psi$$
$$\theta\mu(\beta_p + \beta_D)L^{13} \cos\psi]$$

$$A_{34} = -\left(\bar{\omega}_{L1}^2 - \frac{\bar{\bar{E}}^s}{\bar{M}_{L1}} \right) + \frac{\gamma}{2} \left(\frac{\ell}{R} \right)^2 \left\{ -\theta\lambda\mu L^{20}\cos\psi + \frac{\mu^2}{2}(1 \right.$$
$$+\cos 2\psi)[-L^{21}g_1^o - (\beta_p + \beta_D)L^{20}]\theta + \frac{C_{Do}}{a}(-\mu^2 L^{20} \sin 2\psi$$
$$- 2\mu L^{23} \cos\psi) \Big\}$$

where

$$X_H = \frac{2\bar{P}_{111}g_1^o}{\bar{M}_{F1}} - \frac{\gamma}{2\bar{M}_{F1}}(\frac{\ell}{R})^3[2\theta F^{10}-F^{11}\lambda]+\frac{\bar{B}^3}{\bar{M}_{F1}}2(\beta_P+\beta_D)$$

$$Y_G = -\frac{2(M_\eta)_{111}g_1^o}{\bar{M}_{L1}} + \frac{\gamma}{2\bar{M}_{L1}}(\frac{\ell}{R})^3[L^7\theta-2\lambda L^8]-\frac{\bar{B}^7}{\bar{M}_{L1}}2(\beta_P+\beta_D)$$

Appendix C. Approximate Reverse Flow Model and the Associated Aerodynamic Loads

The circular region of reversed flow, which exists over the retreating blade, is quite well known. In past treatments of reversed flow it has been customary[3] to define three separate regions: (a) normal flow, (b) reversed flow, (c) mixed flow, and evaluate the appropriate aerodynamic expressions for each region. When this model is used together with a modal representation of the blade the evaluation of the generalized aerodynamic expressions F^i, L^i becomes quite cumbersome, and a more convenient procedure had to be devised.

The approximate reverse flow model developed for the present study consists of replacing the circular region, by an approximate region which is a circular sector as shown in Figure 1. The approximation is based on the assumption that the area contained in the circular sector must be equal to the area contained in the approximate region. Two separate cases must be considered: (1) $\mu < 1$, (2) $\mu \geq 1$.

Case (1). For $\mu < 1$, the radius of the circular part is taken as μ. Simple geometric considerations show that the angle α is always a constant.

given by $\alpha = \pi/2$

Case (2). For $\mu \geq 1$ simple geometric considerations show that

$$\alpha = \pi - 2\sin^{-1}(\frac{1}{\mu}) + \mu^2 \sin^{-1}(\frac{1}{\mu}) - \sqrt{\mu^2-1}$$

Thus, for $\mu < 1$ the generalized aerodynamic loads are calculated from

$$\bar{A}_{Fi} = \frac{\ell^2}{\Omega^2 I_b}\left[-\int_{\bar{A}}^{\mu}L_z\eta_i\,d\bar{x}_o + \int_{\mu}^{\bar{B}}L_z\eta_i\,d\bar{x}_o\right]$$

$$\bar{A}_{Li} = -\frac{\ell^2}{\Omega^2 I_b}\left[-\int_{\bar{A}}^{\mu}L_y\gamma_i\,d\bar{x}_o + \int_{\mu}^{\bar{B}}L_y\gamma_i\,d\bar{x}_o\right]$$

while for $\mu \geq 1.0$

$$\bar{A}_{Fi} = -A_{Fi} \quad \text{and} \quad \bar{A}_{Li} = -A_{Li}$$

These expressions are based on the assumption that the lift curve slope in the reversed flow region is equal to the negative value of the lift curve slope in normal flow.

Figure 1. Displacement Field of a Torsionally Rigid Cantilevered Blade with Droop and Preconing.
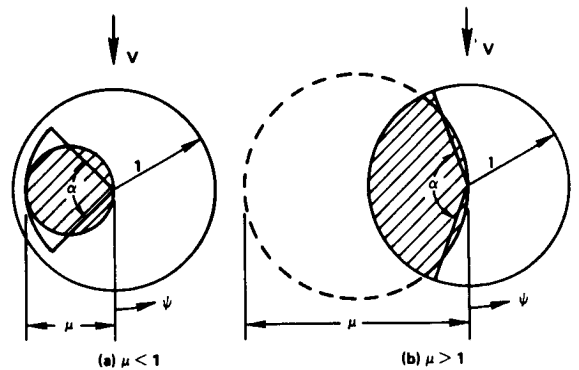
Figure 2. Geometry of Approximate and Exact Reverse Flow Regions.

1. ALL 0 (c_D^3) TERMS IN LAG EQ. NEGLECTED
2. ALL TERMS INCLUDED
3. ONLY 0 (c_D^3) TERMS ASSOCIATED WITH
   DAMPING INCLUDED

$\bar{\omega}_{F1} = 1.175$
$\bar{\omega}_{L1} = 1.28303$
$\gamma = 10.0$
$\sigma = .05$
$\beta_P = 0.0$
$\beta_D = 0.0$
$\theta = .15$
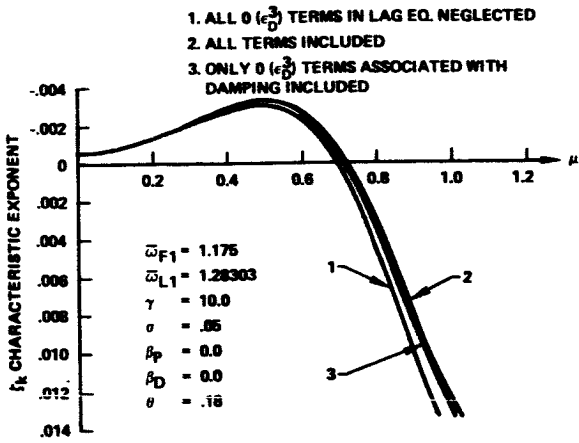
Figure 3. Effect of Third Order Terms in the Lag Equation on Characteristic Exponent for Lag.

$\bar{\omega}_{F1} = 1.175$
$\bar{\omega}_{L1} = 1.28303$
$\gamma = 10.0$
$\sigma = 0.05$
$\beta_P = 0.0$
$\beta_D = 0.0$
$\theta = .15$
$\eta_{SF_1} = .01$
$\eta_{SL_1} = .01$

WITH REVERSE FLOW

WITHOUT REVERSE FLOW
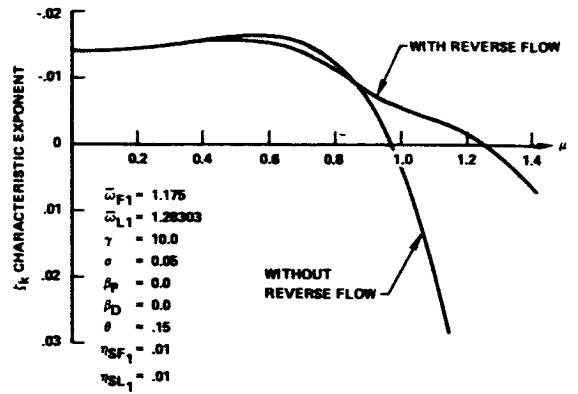
Figure 4. Effect of Reversed Flow on Characteristic Exponent for Lag.

$\bar{\omega}_{F1} = 1.175$
$\bar{\omega}_{L1} = 1.28303$
$\gamma = 10.0$
$\sigma = .05$
$\beta_P = 0.0$
$\beta_D = 0.0$
$\theta = .15$

RADIAL FLOW TERMS INCLUDED

RADIAL FLOW TERMS NOT INCLUDED

ω_k CONTINUOUS
$\omega_k = 0.0$ OR 1.0
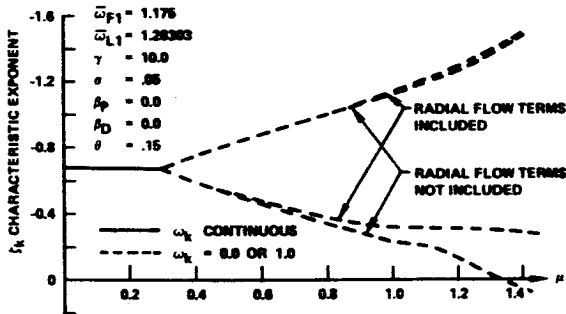
Figure 5. Effect of Radial Flow Terms on Characteristic Exponent for Flap.

$\bar{\omega}_{F1} = 1.175$
$\bar{\omega}_{L1} = 1.28303$
$\gamma = 10.0$
$\sigma = .05$
$\beta_P = 0.0$
$\beta_D = 0.0$
$\theta = .15$

RADIAL FLOW TERMS NOT INCLUDED

RADIAL FLOW TERMS INCLUDED
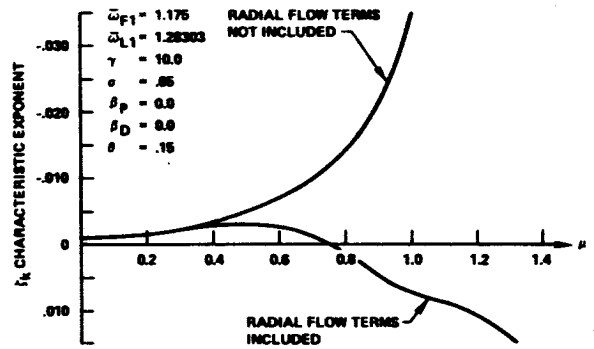
Figure 6. Effect of Radial Flow Terms on Characteristic Exponent for Lag.

$\eta_{SF_1} = \eta_{SL_1} = 0.02$

$\eta_{SF_1} = \eta_{SL_1} = 0.01$

$\bar{\omega}_{F1} = 1.175$
$\bar{\omega}_{L1} = 1.28303$
$\gamma = 10.0$
$\sigma = .05$
$\beta_P = 0.0$
$\beta_D = 0.0$
$\theta = .15$

$\eta_{SF_1} = \eta_{SL_1} = 0.005$
$\eta_{SF_1} = \eta_{SL_1} = 0.0$
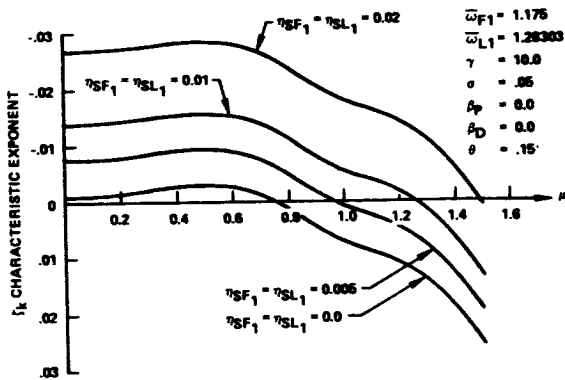
Figure 7. Effect of Viscous Structural Damping on Characteristic Exponent for Lag.

$\bar{\omega}_{F1} = 1.175$
$\bar{\omega}_{L1} = 1.28303$
$\gamma = 10.0$
$\sigma = 0.05$
$\beta_P = 0.0$
$\beta_D = 0.0$
$\theta = .15$

• ELASTIC COUPLING, EXACT MODE SHAPE
▲ NO ELASTIC COUPLING, EXACT MODE SHAPE
■ NO ELASTIC COUPLING, ASSUMED MODE SHAPE
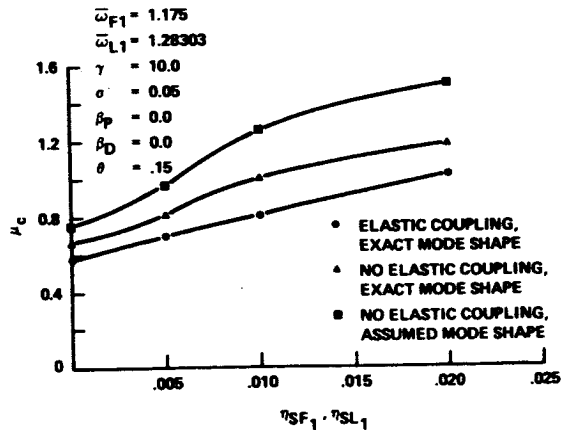
$\eta_{SF_1} \cdot \eta_{SL_1}$

Figure 8. Critical Advance Ratio μ_c vs Structural Damping Coefficients η_{SF_1}, η_{SL_1}.

65
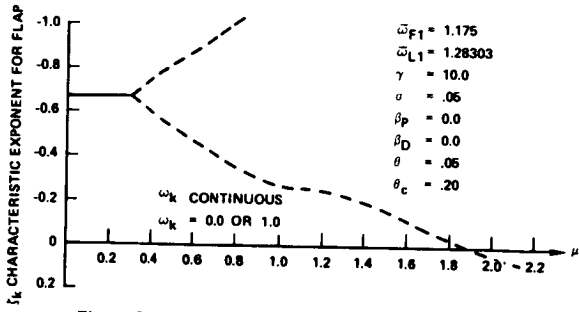
Figure 9. Effect of Collective Pitch on Typical Case.
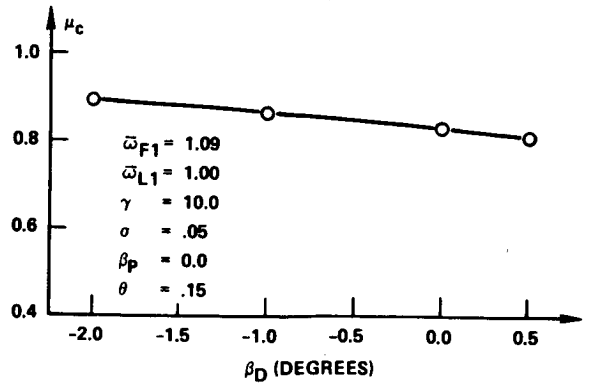
Figure 10. Effect of Droop on μ_c.
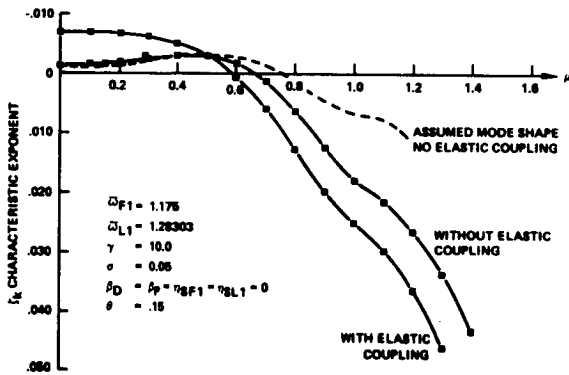
Figure 11. Effect of Exact Mode Shape and Elastic Coupling
on Characteristic Exponent for Lag.